Microscopic flows of a simple yield stress material in the presence of wall slip

E. Younes[a], V. Bertola[b], C. Castelain[c], T. Burghelea[d]

a. Université de Nantes, CNRS, Laboratoire de Thermique et Energie de Nantes, UMR 6607, La Chantrerie, Rue Christian Pauc, B.P. 50609, 44306 Nantes Cedex 3, France. Eliane.Younes@univ-nantes.fr

b. Laboratory of Technical Physics, School of Engineering, University of Liverpool, Liverpool, L69 3GH, United Kingdom. Volfango.Bertola@liverpool.ac.uk

c. Université de Nantes, CNRS, Laboratoire de Thermique et Energie de Nantes, UMR 6607, La Chantrerie, Rue Christian Pauc, B.P. 50609, 44306 Nantes Cedex 3, France. Cathy.Castelain@univ-nantes.fr

d. Université de Nantes, CNRS, Laboratoire de Thermique et Energie de Nantes, UMR 6607, La Chantrerie, Rue Christian Pauc, B.P. 50609, 44306 Nantes Cedex 3, France. Teodor.Burghelea@univ-nantes.fr

Abstract :

*A fundamental problem in the hydrodynamics of yield stress fluids relates to the wall slip phenomenon. To gain insights into this phenomenon, we have performed systematic measurements of steady flows of a simple yield stress fluid (Carbopol Ultrez 10) in a plane acrylic micro-channel. By means of epifluorescent microscopy combined with a custom developed Digital Particle Image Velocimetry (**DPIV**), times series of velocity fields were measured within a wide range of flow rates and three distinct flow regimes were identified: full plug, partial plug and fully yielded. Corresponding to each flow regime, wall velocity gradients and slip velocities were obtained by extrapolating the velocity profiles using a smoothing spline function. Furthermore, by combining the flow field measurements with the macro-rheological measurements, we identified scaling laws of the wall velocity gradient and the slip velocity with the wall shear stress. Finally, we present a detailed comparison of the experimental scaling laws of the wall slip with results from the literature.*

Keywords: Carbopol gel, yield stress, rheology, microchannel, DPIV, wall slip

1 Introduction

Yield stress fluids represent a broad class of materials that naturally exist in a solid state but, if sufficiently forced (e.g. subjected to a large enough stress) they behave as fluids i.e. they flow [1]. Such materials are encountered in everyday life in a variety of forms including pasty materials commonly related to the food industry (e.g. ketchup, mustard, molten chocolate), construction industry (cements), oil industry (drilling oils), cosmetics (toothpaste, hair gel, creams), pharmaceutical industry (drug delivery gel capsules, vertebral repair gels etc.).

Most of the yield stress fluids exhibit a shear thinning behaviour beyond the yield point classically described by the Herschel-Bulkley model:

$$\begin{cases} \sigma = \sigma_y + k|\dot{\gamma}|^n & \text{if} \quad \sigma \geq \sigma_y \\ \dot{\gamma} = 0 & \text{if} \quad \sigma < \sigma_y \end{cases} \tag{1}$$

Here σ is the applied stress, σ_y is the yield stress, $\dot{\gamma}$ is the shear rate, k is the consistency of the material and n is the power law index. This model predicts a solid-fluid transition that occurs at a well defined value of the applied stress (commonly referred to as yield stress).

Carbopol gels have been long considered as a "model" yield stress fluids used to study the yielding behaviour of viscoplastic materials [2]. Carbopol is a cross-linked polyacrylic acid (COO^-H^+) with high molecular weight. In an anhydrous state, it is commercialized in the form of a white powder soluble in aqueous solvents. After addition of a neurtralizing agent such as sodium hydroxide (NaOH), a clear gel is obtained. Such microgels exhibit a viscoplastic rheological behaviour: once the applied stress exceeds a certain threshold, the gel networks break completely and the material starts to flow [3].

For over a decade, it has been considered that Carbopol gels follow the Herschel-Bulkley constitutive model [4, 2]. However, it has been shown recently that the solid-fluid transition does not occur at a well defined value of the applied stress but gradually, i.e. within a finite range of stresses [3, 5]. In the present study, we choose the Carbopol gel as a working fluid because of its chemical stability and optical transparency.

There exists a large number of experimental studies of the flow of Carbopol gels in macroscopic rheometric setups. Rotational rheometers are used to characterise yield stress materials provided that the wall slip is eliminated. The presence of slip on the walls complicates the determination of the yield stress [6] and compromises the assessment of the solid-fluid transition [7]. However, the wall slip phenomenon is ubiquitous during flow of pasty materials.

The study of flow kinematics in a real industrial flows has received limited attention. Ouvrier and Windhab [8] developed a novel rheological technique based on ultrasonic pulsed echo Doppler technique and pressure difference method in order to characterise the flow behaviour of a non-transparent and highly concentrated suspensions in a cylindrical pipe. The local shear stresses were inferred from the measured pressure drop along the pipe and the wall slip velocity was calculated by extrapolating the velocity profile at the wall.

An experimental investigation was carried out by Ma et al. [9]. They proposed a model to determine the rheological properties and the wall slip behaviour of a petroleum-coke sludge slurry flowing in pipelines by using the traditional Mooney method [10] and Tikhonov regularization [11].

A study of the yielding process in a capillary tube of a 0.2 *wt%* Carbopol gel was performed by Pérez-González et al. [12]. By combining the Particle Image Velocimetry technique and classical rheological measurements they found that the solid-fluid transition occurs gradually which complicates the determination of the yield stress. To overcome the difficulty of reliably measuring the yield stress they propose an alternative method based on the analysis of velocity profiles.

An experimental study of unsteady laminar flow of a Carbopol gel were performed by Poumaere et al. [7]. Three distinct flow regimes are observed in both a rheometric and a pipe flow configurations: solid, solid-fluid and fluid.

All the above mentioned studies refer to macroscopic flows. However, there are only few studies that address the wall slip phenomenon at micro-scale where the influence of the confinement is more important and the effects of the slip are more pronounced.

Geraud et al. [13] studied the influence of confinement on the flow of a Carbopol microgel. They compare the bulk rheological behaviour measured with a rheometer and the velocity profiles measured in rough microchannels. They found a strong disagreement between the bulk prediction of the velocity profiles and the ones measured in the micro-channels and they attribute this discrepancy to the confinement of the flow.

Liu et al. [14] compared the measured velocity profiles in micro-channels to simulations performed based on the bulk rheology. They show that the confinement effects are noticeable when the dimensions of the channel are comparable to the characteristic time scale of the material's microstructure.

These two studies address the confinement effects without directly tackling the wall slip which is known to be important in the flow of yield stress fluids. To date, we do not have a clear picture of the wall phenomenon during flow of pasty materials. We present in the current study a detailed experimental investigation of the flow behaviour of a 0.1 $wt\%$ Carbopol gel in an acrylic micro-channel in the presence of wall slip using **DPIV** technique and classical rheological measurements.

The paper is organised as follows. The rheological characterisation of the working fluid is presented in Sec. 2.1. The micro-channel setup design as well as data acquisition are presented in Sec. 2.2. The data analysis procedure is discussed in Sec. 2.3. A detailed characterisation of the velocity profiles is presented in Sec. 3.1. By combining the micro-fluidic and macro-rheological measurements, we identify in Sec. 3.2 different scaling laws of the wall slip phenomenon corresponding to different flow regimes. A detailed comparison of the experimentally found scaling laws with the results from the literature is presented in Sec. 3.3. The paper closes with a summary of the main conclusions and several perspectives, Sec. 4.

2 Experimental methods

2.1 Preparation and rheological characterisation of the working fluid

2.1.1 Fluid preparation

The working fluid was an aqueous solution of 0.1 $wt\%$ Carbopol Ultrez 10. The solution was prepared according to the following protocol. First, the right amount of anhydrous Carbopol was dissolved in deionised water using a magnetic stirring device at a speed of 1000 rpm. The degree of mixing/dissolution was assessed visually by monitoring the optical isotropy of the solution. Next, the pH of the solution was gradually increased from 3.2 to 7 by gradual titration with a small amounts of a 10 $wt\%$ aqueous $NaOH$ solution gradually pipetted while gently mixing the solution. The rheological tests were performed after seeding the Carbopol solution with the fluorescent tracers as detailed in Sec. 2.2. The average density of the Carbopol solution was $\rho_f \approx 1100\ kg.m^{-3}$.

2.1.2 Rheological measurments

The rheological measurements were performed using a controlled stress rotational rheometer (Mars *III*, Thermofischer Scientific) equipped with a nano-torque module. Tests were performed using a parallel plate geometry with a diameter $D = 35\ mm$ and a gap $d = 1\ mm$. To prevent the wall slip, glass paper with an average roughness of 500 μm was glued on each plate. To account for the addition of the glass paper on the rotating plate of the device, inertia was recalibrated. The absence of any wall slip effect was verified by measuring flow curves in subsequent tests performed with several values of the gap and showing that all measurements perfectly overlap. To prevent the evaporation of the solvent during the rheological measurements a thin layer of commercial oil was added to the free meniscus of the sample.

Rheological measurements were performed according to the following protocol. First, the sample was pre-sheared at a constant applied stress larger than the yield stress for 300 s and allowed to relax for another 300 s. Then, to assess the rheological behavior of the Carbopol gel in different deformation regimes, a commonly used rheological tests consisting of loading the material according to an increasing stress ramp was applied to a fluid sample. The duration of each step was $t_0 = 5\ s$ and the data averaging time per stress value was $\delta t_0 = 2\ s$.

To test the reproducibility and quantitatively assess the instrumental error, each rheological measurement was repeated three times with a fresh sample.

The rheological flow curve is illustrated in Fig. 1. Three distinct deformation regimes are observed. For low values of applied stress, the rate of material deformation $\dot{\gamma}$ remains constant. This corresponds to a solid-like behaviour of the material, region **(S)** in Fig. 1. For high values of applied stress (beyond the yield stress), the material becomes fully yielded, region **(F)** in Fig. 1, and its behaviour follows the Herschel-Bulkley fit (Eq. 1), the red line in Fig. 1.

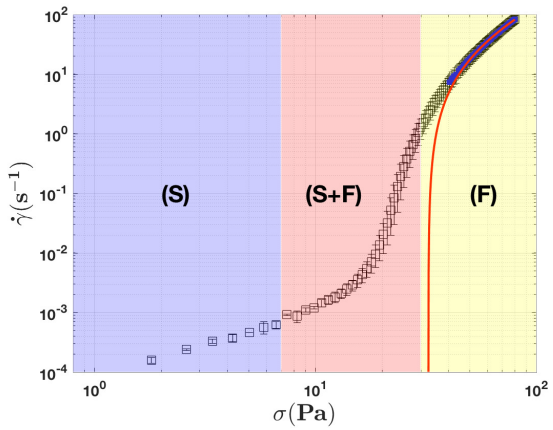

Figure 1: Dependence of the shear rate $\dot{\gamma}$ on the on the applied stress σ. The red line represents the Herschel - Bulkley fit that gives $\sigma_y = 32.5 \pm 2.5\ Pa$, $K = 2.8 \pm 0.215\ Pa.s^n$, $n = 0.6403 \pm 0.0299$. The symbols marking the highlighted regions denote the deformation regimes and are explained in the text: **(S)** - solid, **(S + F)** - solid-fluid coexistence, **(F)** - fluid.

For intermediate values of the applied stresses, the solid- fluid transition is not direct and the behaviour of the material corresponds neither to a solid-like regime nor to a viscous flow regime, region **(S+F)** in Fig. 1. Based on the Herschel-Bulkley fit, the yield stress of the working material is around $\sigma_y \approx 32.5\ Pa$.

2.2 Micro-channel design, microscopic flow control and data acquisition protocol

To characterise the kinematics of a yield stress fluid flow for a wide range of flow rates in the presence of wall slip, micro-fluidic experiments were performed in a plane acrylic micro-channel. The width of the micro-channel was $W = 200\ \mu m$, its depth was $H = 200\ \mu m$ and its length was $L = 4\ cm$. The micro-channel was machined in an acrylic block with the dimensions $5\ cm \times 3\ cm \times 0.5\ cm$.

The micro-channel chip was mounted on an inverted epifluorescent microscope (Axio Observer A1, serial no3832002215.), Fig. 2. The microscopic flows were visualised through a $20X$ magnification objective (Zeiss EC Plan-NEOFLUAR 20x/0,5) with a numerical aperture $NA = 0.35$ and a long working distance $WD = 70\ mm$.

The microscopic flows were generated using a high precision micro-syringe pump (KdScientific, model Legato 110). To insure a steady flow rate Q which was crucial for this study, we used a $10\ ml$ gas tight syringe (Hamilton, model 1010LT). The flows were illuminated by a powerful halogen lamp coupled to the inverted microscope.

To visualise the flow, the working fluid was seeded with a minute amount of buoyant neutral fluorescent tracers with a diameter of $0.92\ \mu m$ (Fluoresbrite Multifluorescent from Polysciences).

For each flow rate, we waited for 5 mins before starting the image acquisition in order to avoid the transient states and then a series of 1000 flow images was acquired with a digital camera. For the experiments where the flow rate did not exceed $10\ \mu L/min$, we used a Prosilica GE camera with 16 bit quantisation (model GE680C from Allied Technologies). The maximal frame rate achievable with this camera is $200\ fps$. During experiments with flow rates $Q \in [10,23]\ \mu L/min$, a Mikrotron camera was used up to a frame rate of $500\ fps$. Images were acquired at the mid-plane of the micro-channel and at the mid-length where the laminar flow is fully developed as the Reynolds numbers are very small ($Re \approx 10^{-9} - 10^{-3}$).

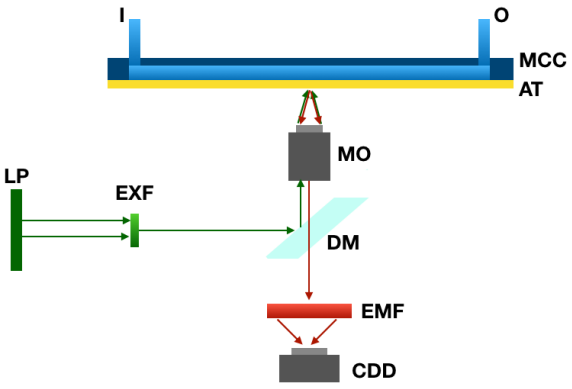

Figure 2: Schematic view of the microfluidic experimental setup: MCC: micro-channel chip, I: micro-channel inlet, O: micro-channel outlet, AT: adhesive tap, MO: microscope objective, DM: dichroic mirror, LP: light emitting lamp, EXF: excitation filter, EMF: emission filter, CCD: digital camera.

2.3 Data analysis

The main tool used to systematically characterise the microscopic flow was an adaptive multi-grid Digital Particle Image Velocimetry (DPIV) (see Refs. [15, 16] for a detailed description of the method) entirely developed in house under Matlab (together with the "Image Processing Toolbox") which followed the steps briefly described below. A background was calculated by averaging all the images of the first time series acquired. Second, the average background was subtracted from images. Finally, pairs of pre-processed images separated in time by the inter-frame t_1 were passed to a multi-pass *DPIV* algorithm using a sequence of square interrogation windows with sizes $[128, 64, 32, 16, 8]$. As a post-processing step, each computed velocity field obtained from the DPIV algorithm was filtered using a median filter. The spatial resolution of the velocity fields was 4.5 μm (44 times smaller than the width of the channel) which suffices for a reliable calculation of the velocity gradients in the proximity of the channel walls.

To extract the slip velocity we extrapolated each transversal profile of the axial velocity by a smoothing spline function and computed its value at the level of the wall. The velocity gradient near the wall was calculated by calculating the slope of the last four points of the smoothing spline.

3 Results

3.1 Description of the flow regimes in the presence of wall slip

We focus in the following on the experimental characterisation of the microscopic flow profiles of a Carbopol gel in a steady channel flow for several flow rates.

Profiles of the time averaged flow velocity U_{av} measured according to the method described in Sec. 2.3 are presented in Fig. 3. Due to the axial symmetry of the flow, velocity profiles were plotted only across half width of the channel ($y = 0$ corresponds to the centreline of the micro-channel and $y = 1 \times 10^{-4}\ m$ corresponds to the channel wall.). The standard deviation of the velocity profiles was smaller than 5% for different values of flow rates. Depending on the magnitude of the constant imposed flow rate Q, three distinct flow regimes are observed in Fig. 3.

At low driving flow rates ($Q < 2\ \mu l/min$), a full plug flow regime is observed in Fig. 3(a). The entire Carbopol gel is un-yielded and "slides" over a very thin liquid layer located in the proximity of the channel walls. The fully plug velocity profiles are characteristic of a solid-like behaviour visible in Fig. 1, region **(S)**.

As the flow rate is gradually increased past this first flow regime, a second flow regime is observed. The Carbopol gel is partially yielded in the proximity of the channel walls (where the velocity gradients are the largest) but a central un-yielded plug may still be observed around the centre-line of the micro-channel, Fig. 3(b). The shear stresses are not large enough to yield the material along the entire width. This behaviour might be related to the solid-fluid transition of the material observed in Fig. 1, region **(S+F)**.

As the flow rate is increased even further ($Q > 10\ \mu l/min$), the Carbopol gel is fully yielded across the entire width of the channel. The further increase of flow rate translates into additional shear stresses and a shear thinning flow regime is observed in Fig. 3(c) (the local shear stresses exceed the yield stress everywhere across the channel width). The shear thinning velocity profiles are characteristic of a fluid-like regime visible in Fig. 1, region **(F)**.

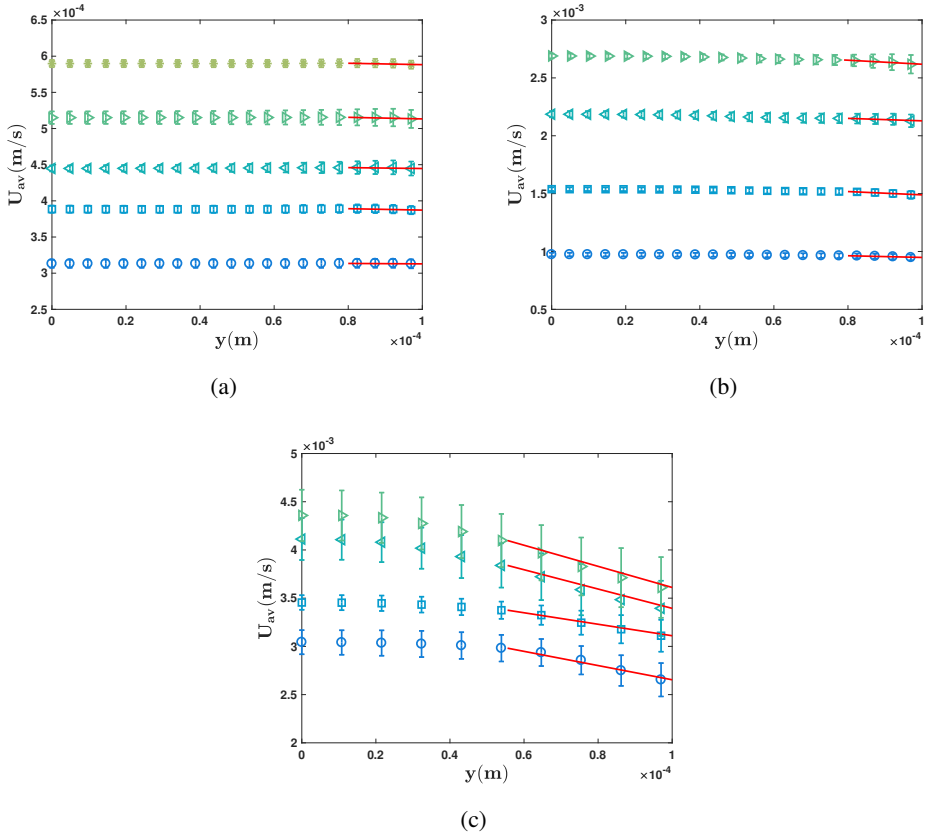

Figure 3: Velocity profiles for different values of flow rate Q. Panel (a) corresponds to the solid regime: circles- $Q = 1\ \mu l/min$, squares- $Q = 1.4\ \mu l/min$, left triangles- $Q = 1.6\ \mu l/min$, right triangles $Q = 1.8\ \mu l/min$, stars- $Q = 2\ \mu l/min$. Panel (b) corresponds to the transition: circles- $Q = 3.5\mu l/min$, squares- $Q = 5.5\ \mu l/min$, left triangles- $Q = 8\ \mu l/min$, right triangles $Q = 10\ \mu l/min$. Panel (c) corresponds to the fluid regime: circles- $Q = 14\ \mu l/min$, squares- $Q = 15\ \mu l/min$, left triangles- $Q = 21\ \mu l/min$, right triangles $Q = 23\ \mu l/min$.

Furthermore, the velocity profiles clearly exhibit a non zero slip behaviour at the channel walls (a non zero slip velocity at $y = 1 \times 10^{-4}\ m$) meaning that the gel slips.

3.2 Scaling behaviour at the wall within various flow regimes

Understanding the scaling behaviour of the relevant hydrodynamic quantities (shear stress, shear rate, slip velocity) in the proximity of the wall is of paramount importance to developing reliable microscopic models able to explain the confined flows of viscoplastic materials in the presence of wall slip and for the implementation of numerical simulations. Based on the characterisation of the flow fields presented in Sec. 3.1, we study in this section the scaling behaviour for each flow regime previously identified.

The dependence of the wall velocity gradients computed according to the procedure detailed in Sec. 2.3 on the flow rate Q is presented in Fig. 4(a). In the solid region **(S)**, the material is fully unyielded and, within the instrumental accuracy of our technique, no velocity gradients could be reliably measured near the solid wall. As the flow rate Q is gradually increased, one can clearly notice the existence of two different scaling regimes. Within the solid-fluid transition regime **(S+F)**, the wall velocity gradient scales with the flow rate as $\frac{dU}{dy}|_w \propto Q^2$ (see full line in Fig. 4(a)). A further increase of the flow rate into

the fluid regime **(F)** leads to a different scaling of the wall velocity gradient, $\frac{dU}{dy}|_w \propto Q^3$ (see dashed line in Fig. 4(a)).

The measurements of the wall velocity gradients $\frac{dU}{dy}|_w$ allow one to compute the wall shear stresses τ_w using the macro-rheological measurements presented in Fig. 1. To do so, we interpreted $\frac{dU}{dy}|_w$ as the relevant scale for the rate of shear and interpolated the corresponding stress from the macro-rheological flow curve. The result of this evaluation is presented in Fig. 4(b). Two different scaling regimes of the wall shear rate with the wall shear stress can be clearly observed. The first scaling regime corresponds to a partial yielding of the gel in the vicinity of the wall, $\frac{dU}{dy}|_w \propto \tau_w^{7.99}$ (see solid line in Fig. 4(b)). Above a critical value of wall shear stress and corresponding to the fluid deformation regime a second scaling regime is observed, $\frac{dU}{dy}|_w \propto \tau_w^{4.8}$ (see dashed line in Fig. 4(b)).

The scaling exponent obtained by fitting the data corresponding to the fully yielded regime differs from the power law exponent obtained by the Herschel-Bullkley fitting to the macro-rheological measurements. This difference might be attributed to the confinement of the flow as suggested in Refs. [13, 14]. However, we can notice that the value of the critical wall shear stress defined as the intersection between the two power laws is close to the yield stress measured in the rheometric flow and fitted by the Herschel-Bulkley model, see Fig. 1.

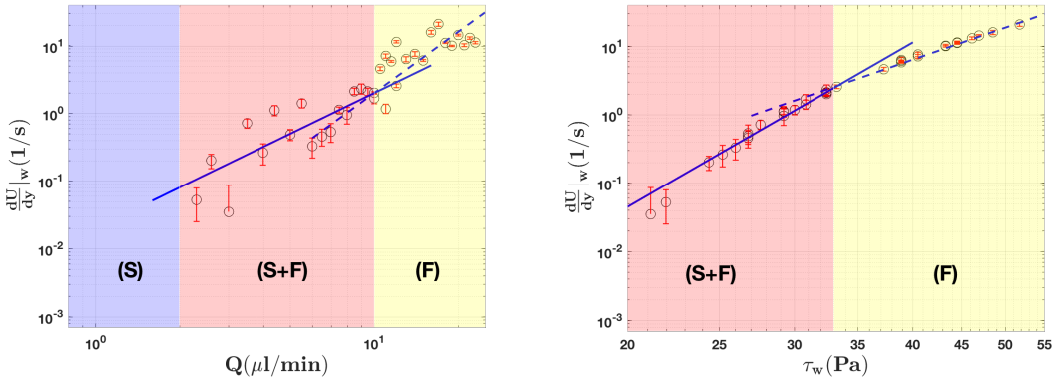

(a) (b)

Figure 4: (a) Dependence of the wall velocity gradient on the applied flow rate Q. The solid line (-) and the dashed line (- -) are guides for the eye, $\frac{dU}{dy}|_w \propto Q^2$ and $\frac{dU}{dy}|_w \propto Q^3$ respectively. (b) Dependence of the wall velocity gradient on the wall shear stress computed using the rheological measurements and computed wall velocity gradients. The solid line (-) and the dashed line (- -) are guides for the eye, $\frac{dU}{dy}|_w \propto \tau_w^{7.99}$ and $\frac{dU}{dy}|_w \propto \tau_w^{4.8}$ respectively.

Wall slip behaviour is usually described as the evolution of the wall slip velocity U_s with the wall shear stress τ_w. This dependence is presented in Fig. 5. Because in the solid regime the wall velocity gradients are too small to be reliably measured, we could not use the method described above to reliably compute the wall shear stresses. For higher flow rates (beyond the **(S)** regime), again, two distinct scaling laws are observed. Corresponding to the solid-fluid coexistence regime **(S+F)**, $U_s \propto \tau_w^{3.55}$. Within the fully yielded flow regime **(F)**, $U_s \propto \tau_w$.

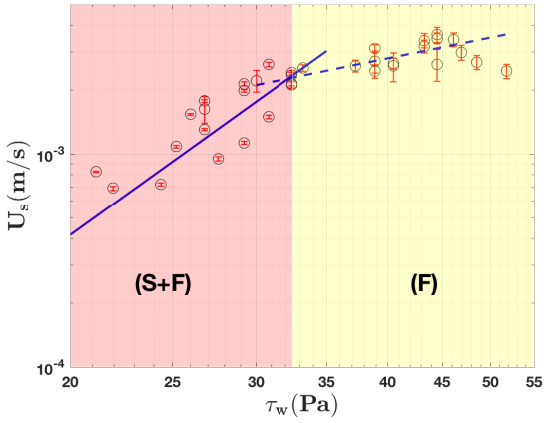

Figure 5: Dependence of the wall slip velocity U_s on the wall shear stress τ_w. The solid (-) and dashed (- -) lines are guides for the eye, $Us \propto \tau_w^{3.55}$ and $Us \propto \tau_w$ respectively.

3.3 Comparison with previous results from the literature

As already stated in the introduction, there exist only very few previous studies of microscopic flows of Carbopol and much more results obtained in macroscopic flows. This will limit the comparison of our results with previous ones.

A study of flow kinematics was carried out by Pérez-González et al. [12]. The apparent shear rate $\dot{\gamma}_a$ and the wall shear stress τ_w were calculated as $\dot{\gamma}_a = \frac{32Q}{\pi D^3}$, $\tau_w = \frac{\Delta P}{4\frac{L}{D}}$ respectively, where ΔP is the pressure drop between the capillary ends, L and D are respectively the length and the diameter of the borosilicate glass capillary and Q is the flow rate calculated from the integration of the velocity profiles. In their study, three distinct flow regimes are observed: a purely plug flow before yielding, solid- liquid transition and shear thinning at relatively high shear rates. The apparent shear rate $\dot{\gamma}_a$ scales with the wall shear stress τ_w as $\dot{\gamma}_a \propto \tau_w^{2.44}$ in the fluid regime. This scaling law differs from the one we observe, $\frac{dU}{dy}|_w \propto \tau_w^{4.8}$ (the dashed line in Fig. 4(b)). This difference might be related to the way $\dot{\gamma}_a$ is calculated ($\dot{\gamma}_a = \frac{32Q}{\pi D^3}$). This formula assumes that the velocity profile is parabolic and the slip is eliminated at the capillary walls.

To describe the wall slip behaviour Kaylon proposed the following relationship between the slip velocity and the wall shear stress [6]:

$$U_s = \beta(\tau_w)^{1/n_b} \tag{2}$$

Here β relates the slip layer δ to the consistency of the binder fluid m_b and to its power-law index n_b, $\beta = \frac{\delta}{m_b^{1/n_b}}$. The Carbopol gel is considered as jammed system of swollen gel micro-particles [2]. As the Carbopol gel was prepared with an aqueous solvent, the "binder fluid" might be considered as Newtonian and thus $K_b = 10^{-3}$ $Pa.s$ and $n_b = 1$.

In the fluid regime, U_s scales linearly with τ_w, $U_s \propto \tau_w$ (the dashed line in Fig. 5). This linear scaling law confirms the assumption that the "binder fluid" is Newtonian, $n_b = 1$. A similar scaling law was found by Poumaere et al. [7] while differs from the ones predicted theoratically by Piau [2] where $U_s \propto \tau_w^{1/3}$ for loosely packed system and $U_s \propto \tau_w^2$ for closely packed system. This difference might be related to the fact that the lubricating fluid is considered as non-Newtonian fluid in Ref. [2] .

In our study, the factor $\beta = 70 \cdot 10^{-6}$ $m.Pa^{-1}.s^{-1}$ leads to a slip layer of thickness $\delta \approx 0.07$ μm. This

value is of the same order of magnitude as the one found by Jiang et al. [17], $\delta \approx 0.1\ \mu m$ and by Poumaere et al. [7], $\delta \approx 0.23\ \mu m$.

By direct observation of a rheometric microgel flow , Meeker et al. in Ref. [18] observe that U_s remains constant for $1 < \frac{\sigma}{\sigma_y} < 1.5$ (σ is the applied stress) while in our experiments the slip velocity increases linearly with the wall shear stress, $Us \propto \tau_w$.

4 Conclusions, outlook

An experimental investigation of the wall slip phenomenon during a steady micro-flow of a Carbopol gel was carried out in this study. By means of digital particle image velocimetry, accurate measurements of the flow fields have been performed in a wide range of flow rates. Depending on the magnitude of the flow rate, three distinct flow regimes are observed. At low driving flow rates, a full plug flow regime is observed, Fig. 3(a). As the flow rate is gradually increased, the Carbopol gel is partially yielded in the proximity of the channel walls but a central un-yielded plug may still be observed around the centre-line of the micro-channel, Fig. 3(b). As the flow rate is increased even further, the Carbopol gel is fully yielded across the entire width of the channel, Fig. 3(c).

Measurements of the velocity profiles allow one to obtain the wall velocity gradients and slip velocities by extrapolating the velocity profiles at the channel walls. We use the dependence between the stress and the rate of shear obtained via classical rotational rheometry and we relate the measured wall velocity gradients to the wall stresses in order to obtain experimentally the scaling laws for the wall slip phenomenon. This procedure has the advantage of making absolutely no assumption on either the flow structure or the rheological behavior of the material. The full plug flow regime may be understood in terms of a solid body of un-yielded gel sliding over a thin layer of depleted solvent expelled from the spongy Carbopol structural units in the vicinity of the solid walls. Moreover, two different scaling laws are observed beyond the solid regime. Within the partial yielded flow regime, the slip velocity U_s scales with τ_w as $U_s \propto \tau_w^{3.55}$ and a linear scaling law of the slip velocity with the wall shear stresses is determined within the fully yielded flow regime, Fig. 5.

The results presented in this study clearly call for future theoretical developments along several main lines. First, to understand the emergence of wall slip, one needs to develop a theoretical physico-chemical framework able to confirm the formation of a depleted layer of the solvent near the wall which in turn would allow one to predict analytical laws for the scaling of the slip velocity with the wall shear stresses. Second, such physical picture of the wall slip could later be incorporated in a novel constitutive law to fully describe the flow of a pasty material along a smooth solid surface.

Acknowledgements

We acknowledge the Agence Nationale de la Recherche (ANR) for the financial support via project NaiMYS (ANR-16-CE06-0003).

References

[1] P. Coussot, Rheometry of pastes, suspensions and granular materials, John Willey & Sons, 2005.

[2] J.M. Piau, Carbopol gels: Elastoviscoplastic and slippery glasses made of individual swollen sponges: Meso- and macroscopic properties, constitutive equations and scaling laws, Journal of Non-Newtonian Fluid Mechanics, 144 (2007) 1-29.

[3] A. M. V. Putz and T. I. Burghelea, The solid-fluid transition in a yield stress shear thinning physical gel, Rheol Acta, 48 (2009) 673-689.

[4] S. J. Curran, R. E. Hayes, A. Afacan, M. C. Williams and P. A. Tanguy, Properties of Carbopol Solutions as Models for Yield-Stress Fluids, Journal of Food Science, 67 (2002) 176-180,

[5] T. Divoux, D. Tamarii, C. Barentin and S. Manneville, Transient Shear Banding in a Simple Yield Stress Fluid, Phys. Rev. Lett., 104 (2010) 208-301.

[6] D. M. Kalyon, Apparent slip and viscoplasticity of concentrated suspensions, Journal of Rheology, 49 (2005) 621-640.

[7] A. Poumaere, M. Moyers-Gonzalez, C. Castelain and T. Burghelea Unsteady laminar flows of a Carbopol gel in the presence of wall slip ", Journal of Non-Newtonian Fluid Mechanics ", 205 (2014) 28-40.

[8] B. Ouriev and E. Windhab, Rheological study of concentrated suspensions in pressure-driven shear flow using a novel in-line ultrasound Doppler method, Experiments in Fluids, 32 (2002) 204-211.

[9] X. Ma and Y. Duan and H. Li, Wall slip and rheological behavior of petroleum-coke sludge slurries flowing in pipelines, Powder Technology, 230 (2012) 127-133.

[10] M. Mooney, Explicit Formulas for Slip and Fluidity, Journal of Rheology, 2 (1931) 210-222.

[11] C. Groetsch, The theory of Tikhonov regularization for Fredholm equations of the first kind, (1984).

[12] J. Pérez-González, J. López-Durán, B. Marín-Santibáñez and F. Rodríguez-González, Rheo-PIV of a yield-stress fluid in a capillary with slip at the wall, Rheologica Acta, 51 (2012) 937-946.

[13] B. Geraud, L. Bocquet and C. Barentin, Confined flows of a polymer microgel, The European Physical Journal E, 36 (2013) 30.

[14] Y. Liu, D. Lorusso, D. W. Holdsworth, T. L. Poepping and J. R. de Bruyn, Effect of confinement on the rheology of a yield-stress fluid, Journal of Non-Newtonian Fluid Mechanics, 261 (2018) 25-32.

[15] F. Scarano and M. L. Rhiethmuller, Advances in iterative multigrid PIV image processing, Exp. Fluids, 29 (2001).

[16] M. Raffel, C. E. Willert, S. T. Wereley and J. Kompenhans, Particle Image Velocimetry: A Practical Guide (Experimental Fluid Mechanics), (2007).

[17] T. Q. Jiang, A. C. Young, and A. B. Metzner, The rheological characterization of HPG gels: Measurement of slip velocities in capillary tubes, Rheologica Acta, 25 (1986) 397-404.

[18] Steven P. Meeker and Roger T. Bonnecaze and M. Cloitre, Slip and flow in pastes of soft particles: Direct observation and rheology, Journal of Rheology, 48 (2004) 1295-1320.